

# The dynamics of starvation and recovery

2 Justin D. Yeakel \* † ‡ §, Christopher P. Kempes † ‡, and Sidney Redner † ¶ ‡

3 \*School of Natural Science, University of California Merced, Merced, CA, †The Santa Fe Institute, Santa Fe, NM, ¶Department of Physics, Boston University, Boston  
4 MA, ‡Contributed equally, and §To whom correspondence should be addressed: jdyeakel@gmail.com

5 Submitted to Proceedings of the National Academy of Sciences of the United States of America

6 The eco-evolutionary dynamics of species are fundamentally  
7 linked to the energetic constraints of its constituent individuals.  
8 Of particular importance are the tradeoffs between reproduction  
9 and the dynamics of starvation and recovery in resource-limited  
10 environments. To elucidate the consequences of this tradeoff,  
11 we introduce a minimal nutritional state-structured model that in-  
12 corporates two classes of consumer: nutritionally replete con-  
13 sumers that reproduce, and undernourished, non-reproducing  
14 consumers that are susceptible to mortality. As a function of the  
15 transition rates between these two states that are determined by  
16 the abundance of resources, the consumer populations can either  
17 undergo cyclic dynamics or reach a steady state. We obtain strong  
18 constraints on starvation and recovery rates by deriving allomet-  
19 ric scaling relationships between body size and a variety of traits  
20 and find that population dynamics subject to these constraints  
21 are typically driven to a steady state. Moreover, we find that these  
22 rates fall within a ‘refuge’ in parameter space, where the probabili-  
23 ty of extinction of the consumer population is minimized. Thus  
24 we identify a potential mechanism that may both drive and con-  
25 strain the dynamics of animal populations. Our model provides a  
26 natural framework that predicts maximum body size for mammals  
27 by determining the relative stability of an otherwise homogeneous  
28 population to a mutant population with altered percentage of body  
29 fat. For body masses  $\lesssim 10^7$  g, individuals with increased energetic  
30 reserves can invade resident populations, and vice versa for body  
31 mass  $\gtrsim 10^7$  g, thus providing a principled mechanism for a within-  
32 lineage driver of Cope’s rule.

33 foraging | starvation | reproduction

34 **Significance Statement** Energetic investment in somatic mainte-  
35 nance and growth vs. reproduction directly impacts the dynamics of  
36 populations among species. Here, we construct a Nutritional State-  
37 structured Model (NSM) to assess the population-level effects of starv-  
38 ation and recovery of a consumer population in a resource-limited en-  
39 vironment, and use allometric scaling relationships for mammals to es-  
40 tablish all timescales and rates. Our model: i. reveals that mammalian  
41 energetic rates minimize the probability of stochastic extinction, ii. es-  
42 tablishes dynamic bounds on mammalian body size while providing  
43 independent theoretical support for the energy equivalence hypothesis,  
44 and iii. provides a mechanistic driver for the evolutionary trend towards  
45 larger body size known as Cope’s rule.

## 46 Introduction

47 The behavioral ecology of all organisms is influenced by the en-  
48 ergic state of individuals, which directly influences how they  
49 invest reserves in uncertain environments. Such behaviors are  
50 generally manifested as tradeoffs between investing in somatic  
51 maintenance and growth, or allocating energy towards repro-  
52 duction (1–3). The timing of these behaviors responds to se-  
53 lective pressure, as the choice of the investment impacts future  
54 fitness (4–6). The influence of resource limitation on an or-  
55 ganism’s ability to maintain its nutritional stores may lead to  
56 repeated delays or shifts in reproduction over the course of an  
57 organism’s life.

58 The balance between (a) somatic growth and maintenance,  
59 and (b) reproduction depends on resource availability (7). For  
60 example, reindeer invest less in calves born after harsh winters  
61 (when the mother’s energetic state is depleted) than in calves  
62 born after moderate winters (8). Many bird species invest dif-  
63 ferently in broods during periods of resource scarcity compared

64 to normal periods (9, 10), sometimes delaying or even foregoing  
65 reproduction for a breeding season (1, 11, 12). Even fresh-  
66 water and marine zooplankton have been observed to avoid  
67 reproduction under nutritional stress (13), and those that do  
68 reproduce have lower survival rates (2). Organisms may also  
69 separate maintenance and growth from reproduction over space  
70 and time: many salmonids, birds, and some mammals return to  
71 migratory breeding grounds to reproduce after one or multiple  
72 seasons in resource-rich environments where they accumulate  
73 nutritional reserves (14–16).

74 Physiology also plays an important role in regulating repro-  
75 ductive expenditures during periods of resource limitation. The  
76 data collected thus far has shown that diverse mammals (47  
77 species in 10 families) exhibit delayed implantation, whereby  
78 females postpone fetal development (blastocyst implantation)  
79 until nutritional reserves can be accumulated (17, 18). Many  
80 other species (including humans) suffer irregular menstrual cy-  
81 cling and higher abortion rates during periods of nutritional  
82 stress (19, 20). In the extreme case of unicellular organisms,  
83 nutrition is unavoidably linked to reproduction because the nu-  
84 tritional state of the cell regulates all aspects of the cell cycle  
85 (21). The existence of so many independently evolved mech-  
86 anisms across such a diverse suite of organisms highlights the im-  
87 portance and universality of the fundamental tradeoff between  
88 somatic and reproductive investment. However the general dy-  
89 namic implications of these constraints are unknown.

90 Though straightforward conceptually, incorporating the en-  
91 ergic dynamics of individuals (22) into a population-level  
92 framework (22, 23) presents numerous mathematical obsta-  
93 cles (24). An alternative approach involves modeling the  
94 macroscale relations that guide somatic versus reproductive  
95 investment in a consumer-resource system. For example,  
96 macroscale Lotka-Volterra models assume that the growth rate  
97 of the consumer population depends on resource density, thus  
98 implicitly incorporating the requirement of resource availability  
99 for reproduction (25).

100 In this work, we adopt an alternative approach in which we  
101 explicitly account for resource limitation and the subsequent  
102 effects of starvation. Namely, only individuals with sufficient  
103 energetic reserves can reproduce. Such a constraint leads to  
104 reproductive time lags due to some members of the population  
105 going hungry and then recovering. Additionally, we incorporate  
106 the idea that reproduction is strongly constrained allometrically  
107 (3), and is not generally linearly related to resource density. As  
108 we shall show, these constraints influence the ensuing popula-

## Reserved for Publication Footnotes

109 tion dynamics in dramatic ways.

110  
111 **Nutritional state-structured model (NSM)**  
112 We begin by defining a minimal Nutritional State-structured  
113 population Model (NSM), where the consumer population is  
114 partitioned into two states: (a) an energetically replete (full)  
115 state  $F$ , where the consumer reproduces at a constant rate  $\lambda$   
116 and does not die from starvation, and (b) an energetically defi-  
117 cient (hungry) state  $H$ , where the consumer does not reproduce  
118 but dies by starvation at rate  $\mu$ . The underlying resource  $R$   
119 evolves by logistic growth with an intrinsic growth rate  $\alpha$  and  
120 a carrying capacity  $C$ . The rate at which consumers transition  
121 between states and consume resources is dependent on their  
122 overall abundance, the abundance of resources, the efficiency of  
123 converting resources into metabolism, and how that metabolism  
124 is partitioned between maintenance and growth purposes. In  
125 the supplementary information (SI) we provide a fully mechani-  
126 stic model for each of these dynamics and constants, and show  
127 that the system produces a simple non-dimensional form which  
128 we describe below.

129 Consumers transition from the full state  $F$  to the hungry  
130 state  $H$  at a rate  $\sigma$ —the starvation rate—and also in proportion  
131 to the absence of resources ( $1 - R$ ) (see SI for detailed descrip-  
132 tion and derivation of all rates and dependencies). Conversely,  
133 consumers recover from state  $H$  to state  $F$  at rate  $\xi\rho$  and in  
134 proportion to  $R$ , where  $\xi$  represents a ratio between maximal  
135 resource consumption and the carrying capacity of the resource.  
136 Resources are eaten by the hungry consumers at rate  $\rho R + \delta$ ,  
137 that accounts for their somatic growth ( $\rho R$ ) and maintenance  
138 ( $\delta$ ). Full consumers eat resources at a constant rate  $\beta$  that  
139 accounts for maximal maintenance and somatic growth (please  
140 see SI for a mechanistic derivation of these terms from resource  
141 energetics). The NSM represents an ecologically motivated fun-  
142 damental extension of the idealized starving random walk model  
143 of foraging, which focuses on resource depletion, to include re-  
144 production and resource replenishment (26–28), and is a more  
145 general formulation than previous models incorporating starva-  
146 tion (29).

In the mean-field approximation, in which the consumers and resources are perfectly mixed, their densities evolve according to the rate equations

$$\begin{aligned} \frac{dF}{dt} &= \lambda F + \xi\rho RH - \sigma(1 - R)F, \\ \frac{dH}{dt} &= \sigma(1 - R)F - \xi\rho RH - \mu H, \\ \frac{dR}{dt} &= \alpha R(1 - R) - (\rho R + \delta)H - \beta F \end{aligned}$$

147 This system of nondimensional equations follows from a set 202 of first-principle relationships for resource consumption and 148 growth (see SI for a full derivation and the dimensional form). 203 Notice that the total consumer density  $F + H$  evolves accord- 149 ing to  $\frac{dF}{dt} + \frac{dH}{dt} = \lambda F - \mu H$ . This resembles the equation of 204 motion for the predator density in the classic Lotka-Volterra 150 model (30), except that the resource density does not appear in 205 the growth term. As discussed above, the attributes of repro- 151 duction and mortality have been explicitly apportioned to the 206 full and hungry consumers, respectively, so that the growth in 152 the total density is decoupled from the resource density. 207

Equation [1] has three fixed points: two trivial fixed points 213 at  $(F^*, H^*, R^*) = (0, 0, 0)$  and  $(0, 0, 1)$ , and one non-trivial, 214

internal fixed point at

$$\begin{aligned} F^* &= \frac{(\sigma - \lambda)\alpha\lambda\mu^2(\mu + \xi\rho)}{A(\lambda\rho B + \mu\sigma(\beta\mu + \lambda(\delta + \rho)))}, \\ H^* &= \frac{(\sigma - \lambda)\alpha\lambda^2\mu(\mu + \xi\rho)}{A(\lambda\rho B + \mu\sigma(\beta\mu + \lambda(\delta + \rho)))}, \\ R^* &= (\sigma - \lambda)\frac{\mu}{A}. \end{aligned} \quad [2]$$

158 where  $A = (\lambda\xi\rho + \mu\sigma)$  and  $B = (\beta\mu\xi + \delta\lambda\xi - \lambda\mu)$ . The sta-  
159 bility of this fixed point is determined by the Jacobian matrix  
160  $\mathbf{J}$ , where each matrix element  $J_{ij} = \partial\dot{X}_i/\partial X_j$  when evaluated  
161 at the internal fixed point, and  $\dot{\mathbf{X}}$  is the vector  $(F, H, R)$ . The  
162 parameters in Eq. [1] are such that the real part of the largest  
163 eigenvalue of  $\mathbf{J}$  is negative, so that the system is stable with  
164 respect to small perturbations from the fixed point. Because  
165 this fixed point is unique, it is the global attractor for all pop-  
166 ulation trajectories for any initial condition where the resource  
167 and consumer densities are both nonzero.

168 From Eq. [2], an obvious constraint on the NSM is that  
169 the reproduction rate  $\lambda$  must be less than the starvation rate  
170  $\sigma$ , so that  $R^*$  is positive. In fact, when the resource density  
171  $R = 0$ , the rate equation for  $F$  gives exponential growth of  
172  $F$  for  $\lambda > \sigma$ . The condition  $\sigma = \lambda$  represents a transcriti-  
173 cal (TC) bifurcation (31) that demarcates a physical from an  
174 unphysical regime where all densities become less than zero.  
175 The biological implication of the constraint  $\lambda < \sigma$  has a simple  
176 interpretation—the rate at which a macroscopic organism loses  
177 mass due to lack of resources is generally much faster than the  
178 rate of reproduction. As we will discuss below, this inequality  
179 is a natural consequence of allometric constraints (3) for organ-  
180 isms within empirically observed body size ranges.

181 In the physical regime of  $\lambda < \sigma$ , the fixed point [2] may  
182 either be a stable node or a limit cycle (Fig. 1). In continuous-  
183 time systems, a limit cycle arises when a pair of complex con-  
184 jugate eigenvalues crosses the imaginary axis to attain positive  
185 real parts (32). This Hopf bifurcation is defined by  $\text{Det}(\mathbf{S}) = 0$ ,  
186 with  $\mathbf{S}$  the Sylvester matrix, which is composed of the coef-  
187 ficients of the characteristic polynomial of the Jacobian ma-  
188 trix (33). As the system parameters are tuned to be within  
189 the stable regime, but close to the Hopf bifurcation, the ampli-  
190 tude of the transient cycles become large. Given that ecological  
191 systems are constantly being perturbed (34), the onset of tran-  
192 sient cycles, even though they decay with time in the mean-field  
193 description, can increase the extinction risk (35–37).

194 When the starvation rate  $\sigma \gg \lambda$ , a substantial fraction  
195 of the consumers are driven to the hungry non-reproducing  
196 state. Because reproduction is inhibited, there is a low steady-  
197 state consumer density and a high steady-state resource den-  
198 sity. However, if  $\sigma/\lambda \rightarrow 1$  from above, the population is  
199 overloaded with energetically-replete (reproducing) individuals,  
200 thereby promoting oscillations between the consumer and re-  
201 source densities (Fig. 1).

202 Whereas the relation between consumer growth rate  $\lambda$  and  
203 the starvation rate  $\sigma$  defines an absolute bound of biological  
204 feasibility—the TC bifurcation— $\sigma$  also determines the sensitiv-  
205 ity of the consumer population to changes in resource density.  
206 When  $\sigma \gg \lambda$ , the steady-state population density is small,  
207 thereby increasing the risk of stochastic extinction. On the  
208 other hand, as  $\sigma$  decreases, the system will ultimately be poised  
209 either near the TC or the Hopf bifurcation (Fig. 1). If the re-  
210 covery rate  $\rho$  is sufficiently small, the TC bifurcation is reached  
211 and the resource eventually is eliminated. If  $\rho$  exceeds a thresh-  
212 old value, cyclic dynamics will develop as the Hopf bifurcation

<sup>215</sup> **Role of allometry**

<sup>216</sup> While there are no a priori constraints on the parameters in the NSM, most organisms correspond to restricted portions of the parameter space. Here we use allometric scaling relations to constrain the covariation of rates in a principled and biologically meaningful manner. Allometric scaling relations highlight common constraints and average trends across large ranges of body size and species diversity. Many of these relations can be derived from a small set of assumptions and below we describe our framework to determine the covariation of timescales and rates across the range of mammals for each of the key parameters of our model (cf. (38)). We are thereby able to define the regime of dynamics occupied by the entire class of mammals, along with the key differences between the largest and smallest mammals.

<sup>230</sup> Nearly all of the rates described in the NSM are determined by consumer metabolism, which can be used to describe a variety of organismal features (39). The scaling relation between an organism's metabolic rate  $B$  and its body mass  $M$  at reproductive maturity is known to scale as  $B = B_0 M^\eta$  (40), where the scaling exponent  $\eta$  is typically close to 2/3 or 3/4 for metazoans (e.g., (39)), and has taxonomic shifts for unicellular species between  $\eta \approx 1$  in eukaryotes and  $\eta \approx 1.76$  in bacteria (3, 41).

<sup>233</sup> Several efforts have shown how a partitioning of  $B$  between growth and maintenance purposes can be used to derive a general equation for both the growth trajectories and growth rates of organisms ranging from bacteria to metazoans (3, 42–45). This relation is derived from the simple balance condition

$$B_0 m^\eta = E_m \frac{dm}{dt} + B_m m,$$

<sup>244</sup> where  $E_m$  is the energy needed to synthesize a unit of mass,  $B_m$  is the metabolic rate to support an existing unit of mass, and  $m$  is the mass of the organism at any point in its development. This balance has the general solution (3, 46)

$$\left(\frac{m(t)}{M}\right)^{1-\eta} = 1 - \left[1 - \left(\frac{m_0}{M}\right)^{1-\eta}\right] e^{-a(1-\eta)t/M^{1-\eta}},$$

<sup>248</sup> where, for  $\eta < 1$ ,  $M = (B_0/B_m)^{1/(1-\eta)}$  is the asymptotic mass, <sup>249</sup>  $a = B_0/E_m$ , and  $m_0$  is mass at birth, itself varying allometrically (see SI). We now use this solution to define the timescale for reproduction and recovery from starvation (Fig. 2; see (43) for a detailed presentation of these timescales). The time that it takes to reach a particular mass  $\epsilon M$  is given by the timescale

$$\tau(\epsilon) = \ln \left[ \frac{1 - (m_0/M)^{1-\eta}}{1 - \epsilon^{1-\eta}} \right] \frac{M^{1-\eta}}{a(1-\eta)},$$

<sup>254</sup> where we will define values of  $\epsilon$  to describe a set of rates within our model. For the time to reproduce,  $t_\lambda = \tau(\epsilon_\lambda)$ , where  $\epsilon_\lambda$  is the fraction of the asymptotic mass where an organism is reproductively mature and should be close to one (typically  $\epsilon_\lambda \approx 0.95$ ). The growth rate is then given by  $\lambda = \ln(v)/t_\lambda$ , where  $v$  is the number of offspring produced, and for any constant value of  $\epsilon_\lambda$ , this rate will scale as  $\lambda \propto M^{\eta-1}$  for  $M \gg m_0$  (3, 42–45).

<sup>261</sup> The rate of recovery  $\rho = 1/t_\rho$  requires that an organism accrues sufficient tissue to transition from the hungry to the full state. Since only certain tissues can be digested for energy (for example the brain cannot be degraded to fuel metabolism),

<sup>265</sup> we define the rates for starvation, death, and recovery by the timescales required to reach, or return from, specific fractions of the replete-state mass (Fig. 3; see SI, Table I for parameterizations). We define  $m_\sigma = \epsilon_\sigma M$ , where  $\epsilon_\sigma < 1$  is the fraction of replete-state mass where reproduction ceases. This fraction

<sup>271</sup> scales with adult mass. For example, making use of the observation that body fat in mammals scales with overall body size according to  $M_{\text{fat}} = f_0 M^\gamma$  and assuming that once this mass is fully digested the organism starves, this would imply that it follows that the recovery timescale,  $t_\rho$ , is given by simply considering an adjusted starting mass of  $m'_0 = \epsilon_\sigma \epsilon_\lambda M$ , in which case

$$t_\rho = \ln \left[ \frac{1 - (\epsilon_\sigma \epsilon_\lambda)^{1-\eta}}{1 - \epsilon^{1-\eta}} \right] \frac{M^{1-\eta}}{a'(1-\eta)} \quad [6]$$

<sup>279</sup> where  $a' = B_0/E'_m$  accounts for possible deviations in the biosynthetic energetics during recovery (see SI). It should be noted that more complicated ontogenetic models explicitly handle storage (45), whereas this feature is implicitly covered by the body fat scaling in our framework.

<sup>284</sup> To determine the starvation rate,  $\sigma$ , we are interested in the time required for an organism to go from a mature adult that reproduces at rate  $\lambda$ , to a reduced-mass hungry state where reproduction is impossible. For starving individuals we assume that an organism must meet its maintenance requirements by using the digestion of existing mass as the sole energy source. This assumption implies the following simple metabolic balance

$$\frac{dm}{dt} E'_m = -B_m m \quad [7]$$

$$\frac{dm}{dt} = -\frac{a'}{M^{1-\eta}} m \quad [8]$$

<sup>291</sup> where  $E'_m$  is the amount of energy stored in a unit of existing body mass, which differs from  $E_m$ , the energy required to synthesize a unit of biomass (45). Given the replete mass,  $M$ , of an organism, the above energy balance prescribes the mass trajectory of a non-consuming organism:

$$m(t) = M e^{-a't/M^{1-\eta}}. \quad [9]$$

<sup>297</sup> The timescale for starvation is given by the time it takes  $m(t)$  to reach  $\epsilon_\sigma M$ , which gives

$$t_\sigma = -\frac{M^{1-\eta}}{a'} \ln(\epsilon_\sigma). \quad [10]$$

<sup>299</sup> The starvation rate is then  $\sigma = 1/t_\sigma$ , which scales with replete-state mass as  $1/M^{1-\eta} \ln(1 - f_0 M^\gamma/M)$ . An important feature is that  $\sigma$  does not have a simple scaling dependence on  $\lambda$  (Fig. 3), which is important for the dynamics that we later discuss.

<sup>303</sup> The time to death should follow a similar relation, but defined by a lower fraction of replete-state mass,  $m_\mu = \epsilon_\mu M$  where  $\epsilon_\mu < \epsilon_\sigma$ . Suppose, for example, that an organism dies once it has digested all fat and muscle tissues, and that muscle tissue scales with body mass according to  $M_{\text{musc}} = u_0 M^\zeta$ . This gives  $\epsilon_\mu = 1 - (f_0 M^\gamma + u_0 M^\zeta)/M$ . Muscle mass has been shown to be roughly proportional to body mass (47) in mammals and thus  $\epsilon_\mu$  is merely  $\epsilon_\sigma$  minus a constant. The time to go from starvation to death is the total time to reach  $\epsilon_\mu M$  minus the time to starve, or

$$t_\mu = -\frac{M^{1-\eta}}{a'} \ln(\epsilon_\mu) - t_\sigma, \quad [11]$$

<sup>314</sup> Although the rate equations [1] are general, here we focus on parameterizations for terrestrial-bound endotherms, specifically mammals, which range from a minimum of  $M \approx 1\text{g}$  (the Etruscan shrew *Suncus etruscus*) to a maximum of  $M \approx 10^7\text{g}$  (the late Eocene to early Miocene Indricotheriinae). Investigating other classes of organisms would simply involve altering the

metabolic exponents and scalings associate with  $\epsilon$ . Moreover, we emphasize that our allometric equations describe mean relationships, and do not account for the variance associated with individual species.

### Stabilizing effects of allometric constraints

As the allometric derivations of the NSM rate laws reveal, starvation and recovery rates are not independent parameters, and the biologically relevant portion of the phase space shown in Fig. 1 is constrained via covarying parameters. Given the parameters of terrestrial endotherms, we find that the starvation rate  $\sigma$  and the recovery rate  $\rho$  are constrained to lie within a small region of potential values (Fig. 4) for the known range of body sizes  $M$ . We thus find that the dynamics for all mammalian body sizes are confined to the steady-state regime of the NSM and that limit-cycle behavior is precluded. Incorporating uncertainty in allometric parameters (20% variation around the mean; Fig. 4), we find that, for larger  $M$ , the distance to the TC and Hopf bifurcation decreases. These results suggest that small mammals are marginally less prone to population oscillations—

both stable limit cycles and transient cycles—than mammals with larger body size. However, starvation and recovery rates across all values of  $M$  fall squarely in the steady state region at some distance from the Hopf bifurcation. This result suggests that cyclic population dynamics should be rare, particularly in environments where resources are limiting.

It should be noted that previous studies used allometric constraints to explain the periodicity of cyclic populations (48–50), suggesting a period  $\propto M^{0.25}$ . However this relation seems to hold only for some species (51), and potential drivers of variation and systematically different behavior range from predator and/or prey lifespans to competitive dynamics (52, 53). Statistically significant support for the existence of population cycles among mammals is relatively rare, though predominantly based on time series for small mammals (54). However the longer gestational times and increased difficulty in collecting data precludes obtaining similar-quality information for larger organisms.

### Extinction risk

Within our model, higher rates of starvation result in a larger flux of the population to the hungry state. In this state, reproduction is absent, thus increasing the likelihood of extinction. From the perspective of population survival, it is the rate

of starvation relative to the rate of recovery that determines the long-term dynamics of the various species (Fig. 1). We therefore examine the competing effects of cyclic dynamics vs. changes in steady-state density on extinction risk, both as functions of  $\sigma$  and  $\rho$ . To this end, we computed the probability of extinction, where we define extinction as a population trajectory falling below one fifth of the allometrically constrained steady state at any time between  $t = 10^5$  and  $t \leq 10^8$ . This procedure is repeated for 50 replicates of the continuous-time system shown in Eq. 1 for an organism of  $M = 100$  grams. In each replicate the initial densities are chosen to be  $(XF^*, XH^*, R^*)$ , with  $X$  a random variable that is uniformly distributed in  $[0, 2]$ . By allowing the rate of starvation to vary, we assessed extinction risk across a range of values for  $\sigma$  and  $\rho$  between ca.  $10^{-7}$  to  $10^{-3}$ . As expected, higher rates of extinction correlate with both high values of  $\sigma$  if  $\rho$  is small, and high values of  $\rho$  if  $\sigma$  is small. For low values of  $\sigma$  and high values of  $\rho$ , the increased extinction risk results from transient cycles with larger amplitudes as the system nears the Hopf bifurcation (Fig. 5). For high values of  $\sigma$  and low values of  $\rho$ , increased extinction risk arises because of the decrease in the steady-state consumer population density (Figs. 1B, 5). This interplay creates an ‘extinction refuge’, such that for a constrained range of  $\sigma$  and  $\rho$ , extinction probabilities are minimized.

We find that the allometrically constrained values of  $\sigma$  and  $\rho$  fall squarely within the extinction refuge (Fig. 5, white point). These values are close enough to the Hopf bifurcation to avoid low steady-state densities, and far enough away to avoid large-amplitude transient cycles. The feature that allometric values of  $\sigma$  and  $\rho$  fall within this relatively small window supports the possibility that a selective mechanism has constrained the physiological conditions that drive starvation and recovery rates within populations. Such a mechanism would select for organ-

ism physiology that generates appropriate  $\sigma$  and  $\rho$  values that serve to minimize extinction risk. This selection could occur via the tuning of body fat percentages, metabolic rates, and biomass maintenance efficiencies. *To summarize, our finding that the allometrically-determined parameters fall within this low extinction probability region suggests that the NSM dynamics may both drive—and constrain—natural animal populations.*

### Dynamic and energetic barriers to body size

Metabolite transport constraints are widely thought to place strict boundaries on biological scaling (39, 55, 56) and thereby lead to specific predictions on the minimum possible body size for organisms (57). Above this bound, a number of energetic

and evolutionary mechanisms have been explored to assess the

costs and benefits associated with larger body masses, particularly for mammals. One important such example is the *fast-ing endurance hypothesis*, which contends that larger body size, with consequent lower metabolic rates and increased ability to maintain more endogenous energetic reserves, may buffer organisms against environmental fluctuations in resource availability (58). Over evolutionary time, terrestrial mammalian lineages show a significant trend towards larger body size (known as Cope’s rule) (59–62), and it is thought that within-lineage drivers generate selection towards an optimal upper bound of roughly  $10^7$  grams (59), a value that is likely limited by higher extinction risk for large taxa over longer timescales (60). These trends are thought to be driven by a combination of climate change and niche availability (62); however the underpinning energetic costs and benefits of larger body sizes, and how they influence dynamics over ecological timescales, have not been explored. We argue that the NSM provides a suitable framework to explore these issues.

The NSM correctly predicts that species with smaller masses have larger steady-state population densities (Fig. 6A). Moreover, we show that the NSM provides independent theoretical support for the energy equivalence hypothesis and Damuth’s Law (63–65). The energy equivalence hypothesis argues that the total energy use,  $B_{\text{tot}}$ , of a population is constant independent of species size (e.g., (63–65)). This hypothesis is based on observations showing that the steady state abundance,  $N^*$ , of a species is proportional to the inverse of individual metabolism ( $N^* \propto M^{-3/4}/B_0$ ) (e.g., (64, 65)). This relationship implies that  $B_{\text{tot}} = N^*B(M) = Q$ , where  $Q$  is a constant, and has been shown to hold in both mammalian and vascular plant communities (63–65). Figure 6A shows that both  $F^*$  and  $H^*$  scale as  $M^{-\eta}$  over a wide range of organism sizes and Figure 6B shows that  $F^*B$  is nearly constant over this same range. This result is remarkable because it illustrates that the steady state values of the NSM combined with the derived timescales naturally give rise to energy equivalence. Our model shows that the equivalence breaks down at the maximum observed body sizes for mammals, suggesting that this maximum is a hard limit where deviations outside of this range are energetically suboptimal. In the framework of our model, the total metabolic rate of  $F$  and  $H$  becomes infinite at a finite mass, and occur at the same scale where the steady state resources vanish (Fig. 6).

453 This asymptotic behavior is governed by body sizes at which 518 ( $\chi < 0$ ) have lower resource steady state densities, switching  
 454  $\epsilon_\mu$  and  $\epsilon_\lambda$  equal zero causing the timescales to become infinite 519 the advantage for higher values of  $M$ .  
 455 (see Equation 11) and the rates  $\mu$  and  $\lambda$  to equal zero. The 520 The observed switch in susceptibility as a function of  $\chi$  at  
 456  $\mu = 0$  asymptote occurs first when  $f_0 M^{\gamma-1} + u_0 M^{\zeta-1} = 1$ , 521  $M_{\text{opt}} = 1.73 \times 10^7 \text{ g}$  thus serves as an attractor, such that the  
 457 and corresponds to  $(F^*, H^*, R^*) = (0, 0, 0)$ . This point pre- 522 NSM predicts organismal mass to increase if  $M < M_{\text{opt}}$  and  
 458 dicts an upper bound on mammalian body size and occurs at 523 decrease if  $M > M_{\text{opt}}$ . This value is close to but smaller than  
 459  $M_{\text{max}} = 6.54 \times 10^7$ . Moreover,  $M_{\text{max}}$ , which is entirely deter- 524 the asymptotic upper bound for terrestrial mammal body size  
 460 mined by the population-level consequences of energetic con- 525 predicted by the NSM, however it is remarkably close to in-  
 461 straints, is remarkably close to the maximum body size observed 526 dependent estimates of the largest land mammals, the early  
 462 in the North American mammalian fossil record (59), as well as 527 Oligocene *Indricotherium* at ca.  $1.3 \times 10^7 \text{ g}$  and the late Miocene  
 463 the mass predicted from an evolutionary model of body size 528 *Deinotherium* at ca.  $1.74 \times 10^7 \text{ g}$  (61). Additionally, our calcula-  
 464 evolution (60). It should be noted that the asymptotic behav- 529 tion of  $M_{\text{opt}}$  as a function of mass-dependent physiological rates  
 465 ior and predicted upper bound depend only on the scaling of 530 is similar to theoretical estimates of maximum body size (60),  
 466 body composition and are independent of the resource param- 531 and provides independent theoretical support for the observa-  
 467 eters. We also note that the prediction of an asymptotic limit 532 tion of a ‘maximum body size attractor’ for North American  
 468 on mammalian size parallels work on microbial life where an 533 mammals outlined by Alroy (59). While the state of the envi-  
 469 upper and lower bound on bacterial size, and an upper bound 534 ronment, as well as the competitive landscape, will determine  
 470 on single cell eukaryotic size, is predicted from similar growth 535 whether specific body sizes are selected for or against (62), we  
 471 and energetic scaling relationships (3, 66). 536 propose that the dynamics of starvation and recovery described  
 472 We contend that the NSM provides a mechanistic under- 537 in the NSM may provide a general within-lineage mechanism  
 473 standing of the energetic dynamics that give rise to both ob- 538 for the evolution of larger body size among terrestrial mammals.  
 474 served limitations on mammalian body size, as well as the ob- 539 The energetics associated with somatic maintenance,  
 475 served trend towards larger body size over evolutionary time. 540 growth, and reproduction are important elements that influence  
 476 The NSM predicts that the steady state resource density  $R^*$  541 the dynamics of all populations (11). The NSM is a minimal  
 477 decreases with increasing body size of the consumer popula- 542 and general model that incorporates the dynamics of starvation  
 478 tion (Fig. 6C), and classic resource competition theory predicts 543 and recovery that are expected to occur in resource-limited en-  
 479 that the species surviving on the lowest resource abundance will 544 vironments. By incorporating allometric relations between the  
 480 outcompete others (67–69). Thus, the combined NSM steady- 545 rates in the NSM, we found: (i) different organismal masses  
 481 state dynamics and allometric timescales predict that larger 546 have distinct population dynamic regimes, (ii) allometrically-  
 482 mammals have an intrinsic competitive advantage given a com- 547 determined rates of starvation and recovery appear to minimize  
 483 mon resource, but does not offer a within-lineage mechanism by 548 extinction risk, and (iii) the dynamic consequences of these rates  
 484 which larger body sizes are selected for. 549 may introduce additional drivers and hard boundaries on the  
 485 To examine whether the NSM could provide such a mecha- 550 evolution of maximum body size. We suggest that the NSM  
 486 nism, we begin by noting that a theoretical upper bound on 551 offers a means by which the dynamic consequences of energetic  
 487 mammalian body size is given by  $\epsilon_\sigma = 0$ , where mammals 552 constraints can be assessed using macroscale interactions be-  
 488 are entirely composed of metabolic reserves, and this occurs at 553 tween and among species. Future efforts will involve exploring  
 489  $M = 8.3 \times 10^8$ , or 120 times the mass of a male African elephant. 554 the consequences of these dynamics in a spatially explicit frame-  
 490 Next we examine to what extent a more realistic upper bound 555 work, thus incorporating elements such as movement costs and  
 491 to body mass may serve as an evolutionary attractor, thus pro- 556 spatial heterogeneity, which may elucidate additional tradeoffs  
 492 viding a suitable within-lineage mechanism for Cope’s rule. We 557 associated with the dynamics of starvation and recovery.

493 directly assess the susceptibility of an otherwise homogeneous  
 494 population to invasion by a mutated subset of the population  
 495 (denoted by ') where individuals have a modified proportion of  
 496 body fat  $M' = M(1 + \chi)$ . For the allowable values of  $\chi$  the ad-  
 497 justed mass should exceed the amount of body fat,  $1 + \chi > \epsilon_\sigma$ ,  
 498 and the adjusted time to reproduce must be positive, which  
 499 given Equation 5, implies that  $1 - \epsilon_\lambda^{1-\eta}(1 + \chi)^{1-\eta} > 0$ . To-  
 500 gether these conditions imply that  $\chi \in (-f_0 M^{\gamma-1}, 1/\epsilon_\lambda - 1)$   
 501 where the upper bound approximately equals 0.05. The modi-  
 502 fied mass adjusts our model via the altered rates of starvation  
 503  $\sigma(M')$ , recovery  $\rho(M')$ , and the maintenance of both starving  
 504  $\delta(M')$  and full consumers  $\beta(M')$ . Importantly,  $\epsilon_\sigma$ , which deter-  
 505 mines the point along the growth curve that defines the state  
 506 of starved foragers, is assumed to remain unchanged for the  
 507 invader population (see SI for detailed derivations of invader  
 508 rates).

509 To assess the susceptibility of the resident population to  
 510 invasion, we determine which consumer has a lower steady-  
 511 state resource density for a given value of  $\chi$ , again with the  
 512 expectation that populations able to survive on lower resource  
 513 densities have a competitive advantage (67). We find that for  
 514  $M \leq 1.73 \times 10^7 \text{ g}$ , having additional body fat ( $\chi > 0$ ) results in  
 515 lower steady state resource density ( $R^* < R'$ ), such that the  
 516 invader has an intrinsic competitive advantage over the resident  
 517 population. However, for  $M > 1.73 \times 10^7 \text{ g}$ , leaner individuals

## References

1. Martin TE (1987) Food as a Limit on Breeding Birds: A Life-History Perspective. *Annu. Rev. Ecol. Syst.* 18:453–487.
2. Kirk KL (1997) Life-History Responses to Variable Environments: Starvation and Reproduction in Planktonic Rotifers. *Ecology* 78:434–441.
3. Kempes CP, Dutkiewicz S, Follows MJ (2012) Growth, metabolic partitioning, and the size of microorganisms. *PNAS* 109:495–500.
4. Mangel M, Clark CW (1988) *Dynamic Modeling in Behavioral Ecology* (Princeton University Press, Princeton).
5. Mangel M (2014) Stochastic dynamic programming illuminates the link between environment, physiology, and evolution. *B. Math. Biol.* 77:857–877.
6. Yeakel JD, Dominy NJ, Koch PL, Mangel M (2014) Functional morphology, stable isotopes, and human evolution: a model of consilience. *Evolution* 68:190–203.
7. Morris DW (1987) Optimal Allocation of Parental Investment. *Oikos* 49:332.
8. Tveraa T, Fauchald P, Henaug C, Yoccoz NG (2003) An examination of a compensatory relationship between food limitation and predation in semi-domestic reindeer. *Oecologia* 137:370–376.

- 582 9. Daan S, Dijkstra C, Drent R, Meijer T (1988) *Food supply and the annual timing of avian reproduction*. (Springer, New York).
- 583 10. Jacot A, Valcu M, van Oers K, Kempenaers B (2009) Experimental nest site limitation affects reproductive strategies and parental investment in a hole-nesting passerine. *Animal Behaviour* 77:1075–1083.
- 584 11. Stearns SC (1989) Trade-Offs in Life-History Evolution. *Funct. Ecol.* 3:259.
- 585 12. Barboza P, Jorde D (2002) Intermittent fasting during winter and spring affects body composition and reproduction of a migratory duck. *J Comp Physiol B* 172:419–434.
- 586 13. Threlkeld ST (1976) Starvation and the size structure of zooplankton communities. *Freshwater Biol.* 6:489–496.
- 587 14. Weber TP, Ens BJ, Houston AI (1998) Optimal avian migration: A dynamic model of fuel stores and site use. *Evolutionary Ecology* 12:377–401.
- 588 15. Mduma SAR, Sinclair ARE, Hilborn R (1999) Food regulates the Serengeti wildebeest: a 40-year record. *J. Anim. Ecol.* 68:1101–1122.
- 589 16. Moore JW, Yeakel JD, Peard D, Lough J, Beere M (2014) Life-history diversity and its importance to population stability and persistence of a migratory fish: steelhead in two large North American watersheds. *J. Anim. Ecol.* 83:1035–1046.
- 590 17. Mead RA (1989) in *Carnivore Behavior, Ecology, and Evolution* (Springer US, Boston, MA), pp 437–464.
- 591 18. Sandell M (1990) The Evolution of Seasonal Delayed Implantation. *The Quarterly Review of Biology* 65:23–42.
- 592 19. Bulik CM, et al. (1999) Fertility and Reproduction in Women With Anorexia Nervosa. *J. Clin. Psychiatry* 60:130–135.
- 593 20. Trites AW, Donnelly CP (2003) The decline of Steller sea lions *Eumetopias jubatus* in Alaska: a review of the nutritional stress hypothesis. *Mammal Review* 33:3–28.
- 594 21. Glazier DS (2009) Metabolic level and size scaling of rates of respiration and growth in unicellular organisms. *Funct. Ecol.* 23:963–968.
- 595 22. Kooijman SALM (2000) *Dynamic Energy and Mass Budgets in Biological Systems* (Cambridge).
- 596 23. Sousa T, Domingos T, Poggiale JC, Kooijman SALM (2010) Dynamic energy budget theory restores coherence in biology. *Philos. T. Roy. Soc. B* 365:3413–3428.
- 597 24. Diekmann O, Metz JAJ (2010) How to lift a model for individual behaviour to the population level? *Philos. T. Roy. Soc. B* 365:3523–3530.
- 598 25. Murdoch WW, Briggs CJ, Nisbet RM (2003) *Consumer-resource Dynamics*, Monographs in population biology (Princeton University Press).
- 599 26. Benichou O, Redner S (2014) Depletion-Controlled Starvation of a Diffusing Forager. *arXiv*.
- 600 27. Bénichou O, Chupeau M, Redner S (2016) Role of Depletion on the Dynamics of a Diffusing Forager.
- 601 28. Chupeau M, Bénichou O, Redner S (2016) Universality classes of foraging with resource renewal. *Phys. Rev. E* 93:032403.
- 602 29. Persson L, Leonardsson K, De Roos AM, Gyllenberg M, Christensen B (1998) Ontogenetic Scaling of Foraging Rates and the Dynamics of a Size-Structured Consumer-Resource Model. *Theoretical Population Biology* 54:270–293.
- 603 30. Murray JD (2011) *Mathematical Biology: I. An Introduction*, Interdisciplinary Applied Mathematics (Springer New York) Vol. 110.
- 604 31. Strogatz SH (2008) *Nonlinear Dynamics and Chaos*, With Applications to Physics, Biology, Chemistry, and Engineering (Westview Press).
- 605 32. Guckenheimer J, Holmes P (1983) *Nonlinear oscillations, dynamical systems, and bifurcations of vector fields* (Springer, New York).
- 606 33. Gross T, Feudel U (2004) Analytical search for bifurcation surfaces in parameter space. *Physica D* 195:292–302.
- 607 34. Hastings A (2001) Transient dynamics and persistence of ecological systems. *Ecol. Lett.* 4:215–220.
- 608 35. Neubert M, Caswell H (1997) Alternatives to resilience for measuring the responses of ecological systems to perturbations. *Ecology* 78:653–665.
- 609 36. Caswell H, Neubert MG (2005) Reactivity and transient dynamics of discrete-time ecological systems. *Journal of Difference Equations and Applications* 11:295–310.
- 610 37. Neubert M, Caswell H (2009) Detecting reactivity. *Ecology*.  
611 38. Yodzis P, Innes S (1992) Body Size and Consumer-Resource Dynamics. *Am. Nat.* 139:1151–1175.
- 612 39. Brown J, Gillooly J, Allen A, Savage V, West G (2004) Toward a metabolic theory of ecology. *Ecology* 85:1771–1789.
- 613 40. West GB, Woodruff WH, Brown JH (2002) Allometric scaling of metabolic rate from molecules and mitochondria to cells and mammals. *Proc. Natl. Acad. Sci. USA* 99 Suppl 1:2473–2478.
- 614 41. DeLong JP, Okie JG, Moses ME, Sibly RM, Brown JH (2010) Shifts in metabolic scaling, production, and efficiency across major evolutionary transitions of life. *PNAS* 107:12941–12945.
- 615 42. West GB, Brown JH, Enquist BJ (2001) A general model for ontogenetic growth. *Nature* 413:628–631.
- 616 43. Moses ME, et al. (2008) Revisiting a Model of Ontogenetic Growth: Estimating Model Parameters from Theory and Data. <http://dx.doi.org.proxy.lib.sfu.ca/10.1086/679735>
- 617 44. Gillooly JF, Charnov EL, West GB, Savage VM, Brown JH (2002) Effects of size and temperature on developmental time. *Nature* 417:70–73.
- 618 45. Hou C, et al. (2008) Energy Uptake and Allocation During Ontogeny. *Science* 322:736–739.
- 619 46. Bettencourt LMA, Lobo J, Helbing D, Kuhnert C, West GB (2007) Growth, innovation, scaling, and the pace of life in cities. *Proc. Natl. Acad. Sci. USA* 104:7301–7306.
- 620 47. Folland JP, Mc Cauley TM, Williams AG (2008) Allometric scaling of strength measurements to body size. *Eur J Appl Physiol* 102:739–745.
- 621 48. Calder III WA (1983) An allometric approach to population cycles of mammals. *J. Theor. Biol.* 100:275–282.
- 622 49. Peterson RO, Page RE, Dodge KM (1984) Wolves, Moose, and the Allometry of Population Cycles. *Science* 224:1350–1352.
- 623 50. Krukonis G, Schaffer WM (1991) Population cycles in mammals and birds: Does periodicity scale with body size? *J. Theor. Biol.* 148:469–493.
- 624 51. Hendriks AJ, Mulder C (2012) Delayed logistic and Rosenzweig–MacArthur models with allometric parameter setting estimate population cycles at lower trophic levels well. *Ecological Complexity* 9:43–54.
- 625 52. Kendall BE, et al. (1999) Why do populations cycle? A synthesis of statistical and mechanistic modeling approaches. *Ecology* 80:1789–1805.
- 626 53. Höglstedt G, Seldal T, Breistol A (2005) Period length in cyclic animal populations. *Ecology* 86:373–378.
- 627 54. Kendall, Prendergast, Bjornstad (1998) The macroecology of population dynamics: taxonomic and biogeographic patterns in population cycles. *Ecol. Lett.* 1:160–164.
- 628 55. Brown J, Marquet P, Taper M (1993) Evolution of body size: consequences of an energetic definition of fitness. *Am. Nat.* 142:573–584.
- 629 56. West GB, Brown JH, Enquist BJ (1997) A General Model for the Origin of Allometric Scaling Laws in Biology. *Science* 276:122–126.

- 716 57. West GB, Woodruff WH, Brown JH (2002) Allometric scal- 739  
717 ing of metabolic rate from molecules and mitochondria to 740 65. Enquist BJ, Brown JH, West GB (1998) Allometric scal-  
718 cells and mammals. *Proc. Natl. Acad. Sci. USA* 99:2473– 741 742 ing of plant energetics and population density : Abstract :  
719 2478. 743 66. Kempes CP, Wang L, Amend JP, Doyle J, Hoehler T (2016)  
720 58. Millar J, Hickling G (1990) Fasting Endurance and the 743 744 Evolution of Mammalian Body Size. *Funct. Ecol.* 4:5–12.  
721 59. Alroy J (1998) Cope's rule and the dynamics of body 745 746 67. Tilman D (1981) Tests of Resource Competition Theory Us-  
722 mass evolution in North American fossil mammals. *Science* 280:731. 747 ing Four Species of Lake Michigan Algae. *Ecology* 62:802–  
723 724 60. Clauset A, Redner S (2009) Evolutionary Model of Species 748 815.  
725 Body Mass Diversification. *Phys. Rev. Lett.* 102:038103. 749 68. Dutkiewicz S, Follows MJ, Bragg JG (2009) Modeling the  
726 61. Smith FA, et al. (2010) The Evolution of Maximum Body 750 751 coupling of ocean ecology and biogeochemistry. *Global Bio-  
727 Size of Terrestrial Mammals. *Science* 330:1216–1219.* 752 753 69. Barton AD, Dutkiewicz S, Flierl G, Bragg J, Follows MJ  
728 62. Saarinen JJ, et al. (2014) Patterns of maximum body size 752 754 (2010) Patterns of Diversity in Marine Phytoplankton. *Sci-  
729 evolution in Cenozoic land mammals: eco-evolutionary pro- 753 755 ence* 327:1509–1511.  
730 cesses and abiotic forcing. *Proc Biol Sci* 281:20132049– 754  
731 20132049.  
732 63. Damuth J (1987) Interspecific allometry of population den- 755  
733 sity in mammals and other animals: the independence of 756 **ACKNOWLEDGMENTS.** We thank Luis Bettencourt, Jean Philippe Gilbert,  
734 body mass and population energy-use. *Biological Journal 757* 758 Eric Libby, and Seth Newsome for helpful discussions and comments on the  
735 *of the Linnean Society* 31:193–246. 759 manuscript. J.D.Y. was supported by startup funds at the University of California,  
736 64. Allen AP, Brown JH, Gillooly JF (2002) Global Biodiver- 760 Merced, and an Omidyar Postdoctoral Fellowship at the Santa Fe Institute. C.P.K.  
737 sity, Biochemical Kinetics, and the Energetic-Equivalence 761 762 was supported by an Omidyar Postdoctoral Fellowship at the Santa Fe Institute.  
738 760 S.R. was supported by grants DMR-1608211 and 1623243 from the National  
761 Science Foundation, and by the John Templeton Foundation, all at the Santa Fe  
762 Institute.

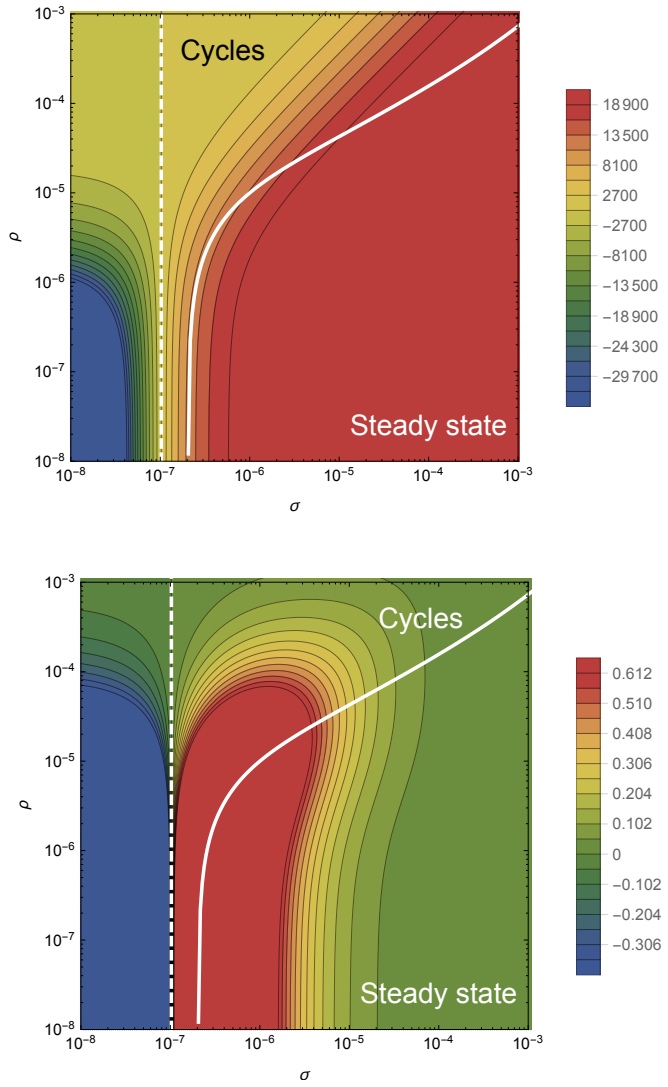


Fig. 1: The transcritical (dashed) and Hopf bifurcation (solid) as a function of the starvation rate  $\sigma$  and recovery rate  $\rho$  for a 100g consumer. These bifurcation conditions separate parameter space into unphysical, cyclic, and steady state dynamic regimes. The colors show the steady state densities for (A) the resource  $R^*$  and the (B) energetically replete consumers  $F^*$ , (warmer colors denote higher densities). Steady state densities for the energetically deficient consumers  $H^*$  (not shown) scale with those for  $F^*$ .

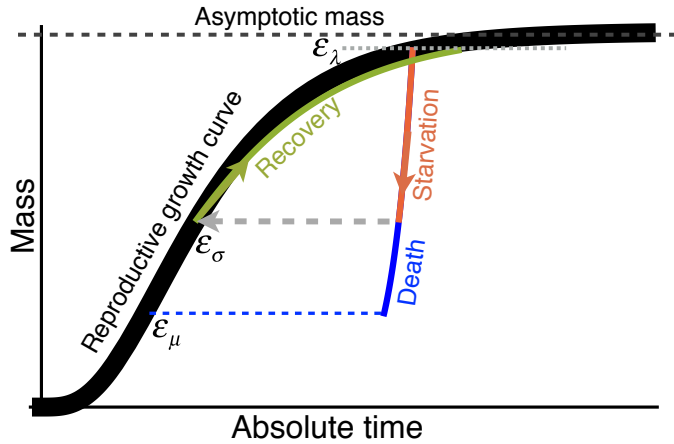


Fig. 2: The growth trajectory over absolute time of an individual organism as a function of body mass. Initial growth follows the black trajectory to an energetically replete reproductive adult mass  $m = \epsilon_\lambda M$  which we assume is 95% asymptotic mass  $M$ . Starvation follows the red trajectory to  $m = \epsilon_\sigma \epsilon_\lambda M$ . Recovery follows the green curve to the replete adult mass, where this trajectory differs from the original growth because only fat is being regrown which requires different energetics and a longer time to reach  $\epsilon_\lambda M$ . Alternatively, death from starvation follows the blue trajectory to  $m = \epsilon_\mu \epsilon_\lambda M$ .

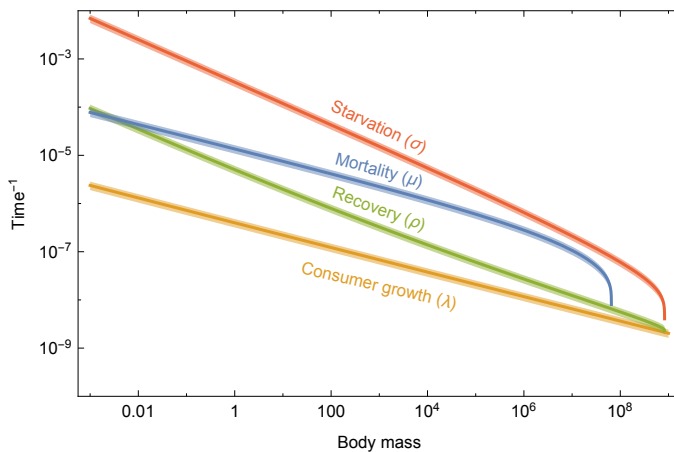


Fig. 3: Allometrically constrained starvation rate  $\sigma = 1/t_\sigma$  (red), mortality  $\mu = 1/t_\mu$  (blue) and recovery rate  $\rho = 1/t_\rho$  (green) relative to the reproductive rate  $\lambda = 1/t_\lambda$  (black) as a function of body mass (see Equations 5, 6, 10, and 11). The rate of starvation is greater than the rate of reproduction for all realized terrestrial endotherm body sizes. Mean values  $\pm 20\%$  variation are shown by the shaded region for each rate.

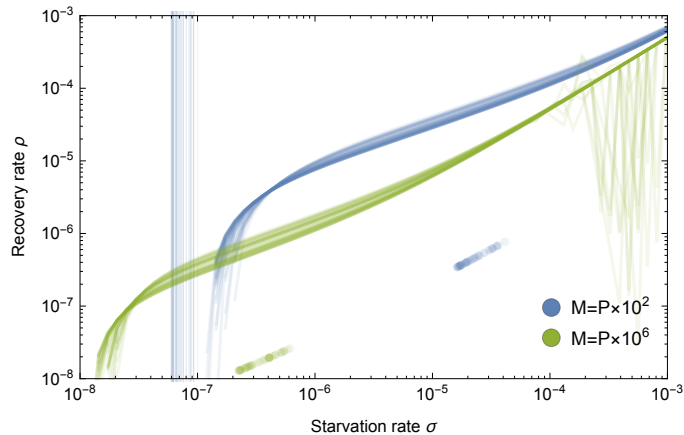


Fig. 4: Transcritical (vertical lines) and Hopf bifurcations (curves) for allometrically determined starvation  $\sigma$  and recovery  $\rho$  rates as a function of different mammalian body sizes:  $M = P \times 10^2 \text{g}$  (blue) and  $M = P \times 10^6 \text{g}$  (green), where  $P$  is a random uniform variable in  $[1, 9]$ . Points denote realized values of  $\sigma$  and  $\rho$  given the drawn values for  $M$ .

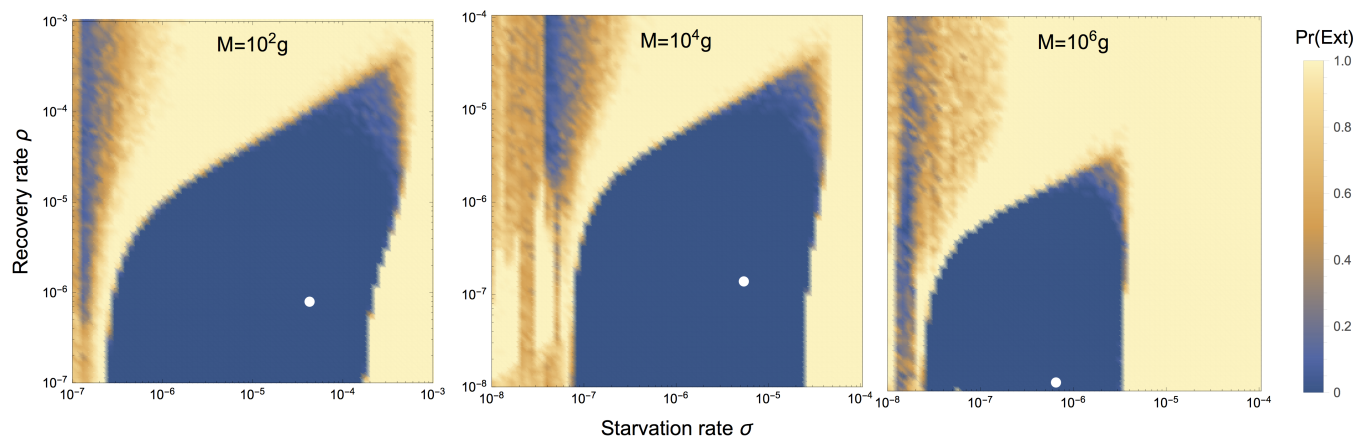


Fig. 5: Probability of extinction for a 100g consumer as a function of the starvation rate  $\sigma$  and recovery rate  $\rho$ , where the initial density is given as  $(XF^*, XH^*, R^*)$ , with  $X$  being a random uniform variable in  $[0, 2]$ . Extinction is defined as the population trajectory falling below 0.1 times the allometrically constrained steady state. The white point denotes the allometrically constrained starvation and recovery rate.

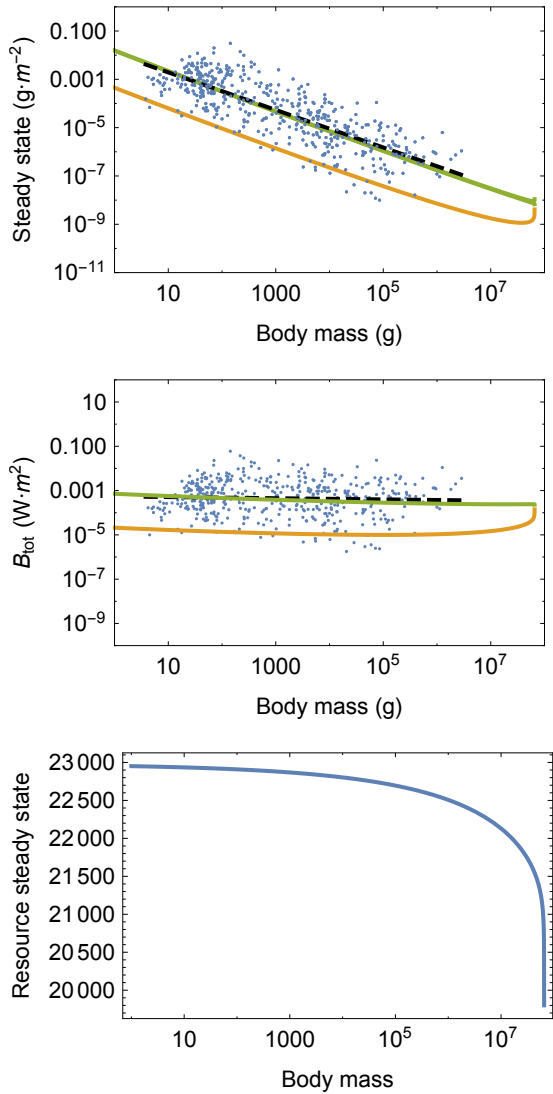


Fig. 6: (A) Consumer steady states  $F^*$  (green) and  $H^*$  (orange) as a function of body mass. (B) Total energetic use  $B_{\text{tot}}$  of consumer populations at the steady state as a function of body mass. (C) Resource steady state  $R^*$  as a function of consumer body mass. The data are from Damuth (63) and have been converted to total population metabolism using the allometric relationships for metabolic rate (please see SI and Refs. (42, 43, 45)).

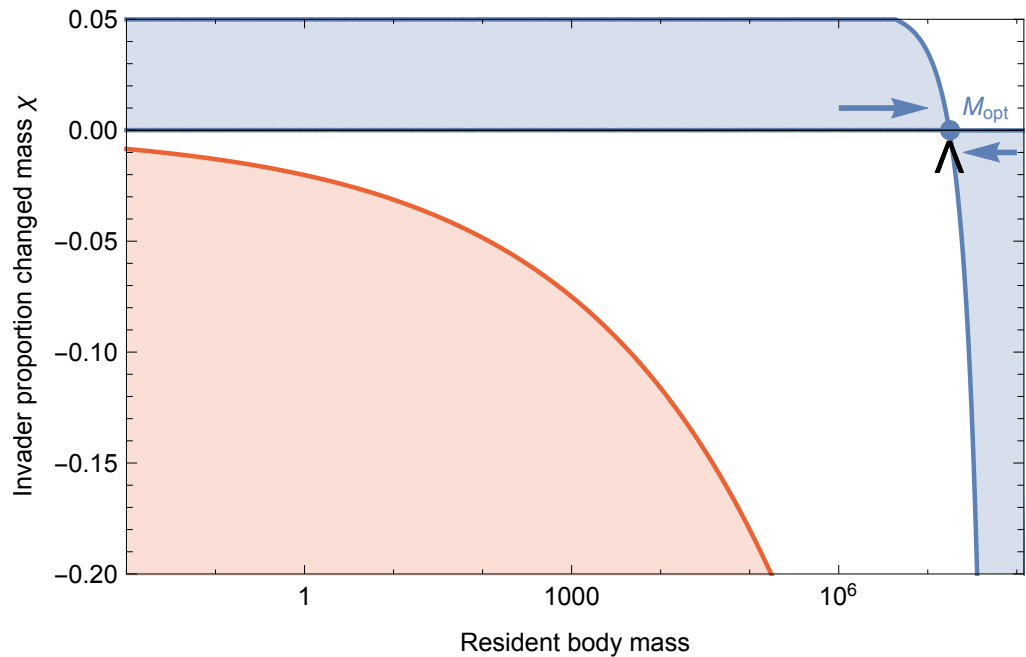


Fig. 7: Invasion feasibility for organisms with a proportional change in mass  $\chi$  against a population with a resident body mass  $M$ . The blue region denotes proportions of modified mass  $\chi$  resulting in successful invasion. The red region denotes values of  $\chi$  that result in a mass that is below the starvation threshold and is thus infeasible. Arrows point to the predicted optimal mass  $M_{\text{opt}} = 1.73 \times 10^7$ , which serves as an evolutionary attractor for body mass. The black wedge points to the largest body mass known for terrestrial mammals at  $7.74 \times 10^7 \text{ g}$  (61).